https://doi.org/10.17113/ftb.58.04.20.6813 original scientific paper

Effect of Ultrasonic Pretreatment on Melon Drying and Computational Fluid Dynamic Modelling of Thermal Profile

Running title: Melon drying and computational fluid dynamic modelling

João Henrique Fernandes da Silva, José Sabino da Silva Neto, Edilene Souza da Silva, Danilo Emídio de Souza Cavalcanti, Patrícia Moreira Azoubel* and Mohand Benachour

Federal University of Pernambuco, Department of Chemical Engineering, Av. Prof. Arthur de Sá, s/n, Cidade Universitária, Recife-PE, 50740-521, Brazil

Received: 22 May 2020
Accepted: 9 November 2020

SUMMARY

Research background. Drying is one of the most traditional processes for food preservation. Optimizing the process can result in a competitive product on price and quality to the market. One technology in use as a pretreatment to drying is ultrasound. This work had as the goal to analyze different drying systems with and without applying ultrasound (US) pretreatment, on heat and mass transfer, simulating numerically the temperature profile by computational fluid dynamics (CFD).

Experimental approach. The melon slices were pretreated with ultrasound for 10 (US10), 20 (US20), and 30 (US30) min at 25 kHz, and the water loss and solids gain were evaluated. Drying was performed at different temperatures (50, 60, and 70 °C). The effective diffusivity was estimated, and experimental data were modeled using empirical models. The airflow in the dryer and the temperature profile in the melon slice were simulated *via* computational fluid dynamics (CFD).

Results and conclusions. Drying time had a 25 % (US20 and US30 at 50 °C) to 40 % (US20 and US30 at 70 °C) reduction. The Two terms model presented the best fit to the experimental data, and the diffusivity coefficients showed a tendency to increase as the time of exposure of the melon to ultrasonic waves increased. Pretreatment water loss and solid gain behavior and drying kinetic and diffusion data were used to choose the best experimental condition to be simulated with CFD. The

*Corresponding author:
Phone.: +558121268583
Fax: +558121267298
E-mail: pazoubel@gmail.com

heat transfer modelling through CFD showed that the temperature distribution along the melon slice was representative. Therefore, the profile obtained via CFD satisfactorily describes the drying process.

Novelty and scientific contribution. The use of simulation tools in real processes allows the monitoring and improvement of existing technologies, such as food drying processes, that involve complex mechanisms, making it difficult to obtain some data. Application of CFD in the drying processes of fruits and vegetables is still very recent, being a field little explored. There is no record in the literature that uses CFD in the drying of melon.

Key words: computational fluid dynamics, melon, ultrasound, drying, heat transfer, mass transfer

INTRODUCTION

Drying is one of the most traditional processes of food preservation. It is widely used for reducing the water content and, so, the water activity, inhibiting or reducing microbial growth and enzymatic reactions, increasing the shelf life without the aid of additives (*1,2*). However, making the product competitive on price, besides quality, is done by optimizing the process, and one technology in use as a pretreatment to drying is ultrasound (*3-11*).

Sound waves, a matter oscillation, propagate mechanically, that is, they need a medium in contact for its propagation. The sound waves have different denominations depending on the type of material that they spread, being denominated "elastic" when they propagate in solids, and "acoustic", when in fluids (*12*). The form of transmission of these waves also varies, that is, when elastic or acoustic. The elastic is transferred as transverse waves, which cause variable shear stress, or longitudinal, causing contraction and intermittent dilatation. The acoustic waves offer only one type of transmission, the longitudinal one (*12,13*). Being the main mechanism caused by the use of ultrasound, acoustic cavitation dominates the tensioactive effects in a liquid system, that is, it acts in the creation, dissemination, and sudden collapse of the bubbles present in the material (*14*). In a solid food with high moisture content, the mass transfer rate (water transport) increases if, in the liquid phase (free water), cavitation occurs, reducing the drying time (*15*).

The drying process presents some difficulties in understanding the mechanisms related to convective heat and turbulent fluid in the exchange zones. Optimizing it is not only to apply synergistic techniques but also to investigate such mechanisms. Therefore, a better understanding of the physical phenomena with the help of predictive tools about convective drying of foods becomes important (16). Among the simulation techniques used, the Computational Fluid Dynamics CFD has been highlighting over the years (*2,16-21*), solving the Navier-Stokes equations using the finite volume method. The

finite volume method solves conservation equations in the physical space by discretizing its integral form. In this method, the domain is subdivided into a finite amount of control volumes from the prerogative that the relevant properties are effectively conserved. In each control volume, a centroid, where the values of each interest variable are calculated, is formed and from this, interpolation is used to calculate the values of each studied property. In this way, an algebraic equation is formulated uniquely for each control (*22*).

Considering the drying process as an important food preservation method, the present work had as aim to study, experimentally, different melon drying conditions with and without ultrasound pretreatment. Also, numerically simulating heat transfer using computational fluid dynamics (CFD) was performed to show the temperature profile in the melon slice.

MATERIAL AND METHODS

Material

Mature melons of the yellow variety (*Cucumis melo* L.) purchased in the local market (Recife-PE, Brazil) were used. The previously selected, washed and peeled raw material was sliced into rectangles (5.0 cm x 3.0 cm x 0.5 cm). The initial moisture (X_0) of the melon, determined by the oven method at 105 °C/24 h (*23*), was 88.61% (wet basis, wb).

Ultrasound pretreatment

Melon samples were weighed, placed in 100 mL beakers containing distilled water, and taken to an ultrasonic bath (Unique, USC-2580A model, Brazil), without mechanical agitation, at approximately 25 °C. Ultrasound application time was 10, 20, and 30 min. The sample/distilled water mass ratio used was 1:4, and the ultrasound frequency was 25 kHz (154 W), according to the literature (*24*). After predetermined times, the samples were taken from the distilled water, placed on absorbent paper for 10 s to remove excess water, and weighed. The stage evaluation was in terms of water loss (WL) and solids gain (SG), calculated using equations 1 and 2, respectively.

$$\mathrm{WL}\ (\%) = \left(\frac{m_{\mathrm{W0}} - m_{\mathrm{Wt}}}{m_0}\right) \cdot 100 \qquad /1/$$

where m_{W0} is the initial water content in the product g), m_{Wt} is the water content in the product at time t (g), and m_0 is the initial mass of the product (g).

$$\mathrm{SG}\ (\%) = \frac{(m_{\mathrm{St}} - m_{\mathrm{S0}})}{m_0} \cdot 100 \qquad /2/$$

where m_{S0} is the initial dry mass (g), m_{St} is the dry mass at time t (g), and m_0 the initial mass of the product (g).

After pretreatment, sample moisture content changed to 90.19 % (wb) for 10-minute ultrasound (US10), 90.74 % (wb) for 20-minute ultrasound (US20), and 90.94 % (wb) for 30-minute ultrasound (US30) pretreated samples.

Drying kinetics

Convective drying of melon slices with and without (control treatment) ultrasound pretreatment was performed at 50, 60, and 70 °C, using a stainless-steel fixed bed dryer (tray dryer) with a fixed air velocity of 2.0 m/s. The choice for the temperature range in this study was to avoid very high drying time (temperatures below 50 °C) and high temperatures, which would cause the loss of nutritional components (temperatures above 70 °C).

Samples were weighed using a semi-analytical balance. The time intervals used for weighing were 15 min during the first hour of drying and 30 min until the equilibrium condition was reached (*10*). The drying kinetics study was performed using dimensionless moisture data. The Fick diffusional model (Equation 3) was used to estimate the effective diffusivity.

$$\frac{\partial X}{\partial t} = D_{\mathrm{eff}} \frac{\partial^2 X}{\partial y^2} \qquad /3/$$

where X is the moisture content (g water/g dry mass), t is the time (s), y is the coordinated direction and D_{eff} is the effective diffusivity of water (m^2/s).

Equation 4 presents the previous equation solution proposed by Crank (25), considering an infinite flat plate, where the effect of shrinkage is not considered, assuming instantaneous thermal equilibrium and moisture on the surface.

$$X_\theta = \frac{X_\mathrm{t} - X_\mathrm{e}}{X_0 - X_\mathrm{e}} = \frac{8}{\pi^2} \sum_{\mathrm{n}=0}^{\infty} \frac{1}{(2\mathrm{n}+1)^2} \exp\left(-(2\mathrm{n}+1)^2 \frac{\pi^2 D_{\mathrm{eff}} t}{4L^2}\right) \qquad /4/$$

where X_θ is the dimensionless moisture, X_t is the mean moisture content at time t (g water/g dry mass), X_e is the equilibrium moisture content (g water/g dry mass), X_0 is the initial moisture content (g water/g dry mass), and L is the half of slab thickness (m).

The linear dependence of the Arrhenius equation, which is a linear function of the logarithm of the diffusivity and the inverse of the temperature, was tested during the drying process using Equation 5.

$$D_{\mathrm{eff}} = A \cdot \exp\left(-\frac{E_\mathrm{a}}{RT}\right) \qquad /5/$$

where E_a is the activation energy (kJ/mol), A is a drying constant, R is the universal gas constant (kJ/(mol·K)), and T is the absolute drying temperature (K).

Modelling of drying kinetics and estimation of thermal properties

Three empirical models were used for drying data fit (*26*):

Two terms (TT):	$X_\theta = a \cdot \exp(-kt) + (1-a) \cdot \exp(-wt)$	/6/
Henderson and Pabis (HP):	$X_\theta = a \cdot \exp(-kt)$	/7/
Page (Pg):	$X_\theta = \exp(-kt^n)$	/8/

where *a*, *k*, *n*, and *w*, are the empirical constants in drying models.

To verify the fit of all the models to the experimental data and their parameters, it was used TIBCO Statistica v. 10.0 (*27*). The determination of the percentage error (E) between the values observed and predicted by the empirical models was done according to Equation 9.

$$\mathrm{E}\,(\%) = \frac{1}{\mathrm{N}}\sum_{\mathrm{i}=1}^{\mathrm{N}}\left|\frac{V_\mathrm{O} - V_\mathrm{P}}{V_\mathrm{O}}\right|_\mathrm{i} 100 \qquad /9/$$

where V_P is the expected value, V_O is the observed value, and N the number of points considered in the curve.

To simulate the temperature profile during the melon drying process, the thermal conductivity (k_p) and specific heat capacity (C_p) were estimated using the equations presented below (*19*). The density (ρ) was calculated using the relation between mass and volume.

Thermal Conductivity (W/(m·K))	$k_\mathrm{p}(\mathrm{X}) = 0.148 + 0.493X$	/10/
Specific heat capacity (J/(kg·K))	$C_\mathrm{p}(\mathrm{X}) = (1.26 + 2.97X) \cdot 1000$	/11/

Simulation of the temperature profile by computational fluidodynamics

The solution of the computational domain was performed using the finite volume method, responsible for solving the Navier-Stokes equations based on conservative principles (*28*). To better observe the current lines acting directly on the heat transfer coefficient, which affects the temperature profile, and considering the geometric domain simplicity, the refining mesh was of high relevance, bringing better precision to the results. The mass transfer study was not possible because the melon (solid domain in this study) should be characterized as a porous domain and this could not be performed. The computational cost to create a mesh that reproduces the pores present in the melon would be too high, making it impractical. Thus, it was performed only the simulation for energy and momentum.

The greatest concentration of mesh elements occurred in-wall and contact regions (such as the air-melon interface), having as a criterion the curvature and proximity of the domains. The generation of the nodes in the mesh elements was done by the Dropped method, which does not generate nodes between the vertices of the geometric element. The fluid domain (air) was represented by an unstructured mesh, due to its importance, which makes use of the Delaunay Triangulation for its generation. However, the solid domain (melon slice) was represented in a structured mesh, because of its geometric simplicity (*29,30*), as shown in Fig. 1.

The trays are not represented in the geometric domain used for simulation since it is composed of a network of fine stainless steel wires, so it was not a perforated plate, which would affect the airflow into the dryer. Such consideration was necessary since the computational cost associated with the mesh refining would be higher. Also, the wires are very thin, so their interference with the airflow can be neglected.

Regarding the considerations made, the effect of shrinkage, the generation of heat inside the product, and radiation effects may be neglected. Thermal properties were considered constant. As for the turbulence, it was considered medium intensity (5 %) and Eddy viscosity ratio (*10*), as its use is recommended when there is no information on the turbulence at the entrance (*30*). The turbulence model used was the SST k–ω (*16,19,28*), justified due to the high Re (>10^4). In the air-dryer and air-slice interfaces, considering conservative heat flux was necessary to give stability to the interface model. The selected flow regime was subsonic, due to the low velocities. This work considered transient regime and incompressible fluid, resulting in the following equations.

Conservation of mass (Law of continuity):

$$\frac{\partial v_x}{\partial x}+\frac{\partial v_y}{\partial y}+\frac{\partial v_z}{\partial z}=0 \qquad /12/$$

Conservation of momentum (Newton's Second Law of Motion):

$$\rho\left(\frac{\partial v_x}{\partial t}+v_x\frac{\partial v_x}{\partial x}+v_y\frac{\partial v_x}{\partial y}+v_z\frac{\partial v_x}{\partial z}\right)=-\frac{\partial p}{\partial x}-\left(\frac{\partial}{\partial x}\tau_{xx}+\frac{\partial}{\partial x}\tau_{yx}+\frac{\partial}{\partial x}\tau_{zx}\right)+\rho g_x \qquad /13/$$

$$\rho\left(\frac{\partial v_y}{\partial t}+v_x\frac{\partial v_y}{\partial x}+v_y\frac{\partial v_y}{\partial y}+v_z\frac{\partial v_y}{\partial z}\right)=-\frac{\partial p}{\partial y}-\left(\frac{\partial}{\partial y}\tau_{xy}+\frac{\partial}{\partial y}\tau_{yy}+\frac{\partial}{\partial y}\tau_{zy}\right)+\rho g_y \qquad /14/$$

$$\rho\left(\frac{\partial v_z}{\partial t}+v_x\frac{\partial v_z}{\partial x}+v_y\frac{\partial v_z}{\partial y}+v_z\frac{\partial v_z}{\partial z}\right)=-\frac{\partial p}{\partial z}-\left(\frac{\partial}{\partial z}\tau_{xz}+\frac{\partial}{\partial z}\tau_{yz}+\frac{\partial}{\partial z}\tau_{zz}\right)+\rho g_z \qquad /15/$$

Conservation of Energy (First Principle of Thermodynamics):

$$\frac{\partial T}{\partial \mathrm{t}} + v_{\mathrm{x}}\frac{\partial T}{\partial \mathrm{x}} + v_{\mathrm{y}}\frac{\partial T}{\partial \mathrm{y}} + v_{\mathrm{z}}\frac{\partial T}{\partial \mathrm{z}} = \frac{k_{\mathrm{P}}}{\rho C_{\mathrm{p}}}\left(\frac{\partial^2 T}{\partial \mathrm{x}^2} + \frac{\partial^2 T}{\partial \mathrm{y}^2} + \frac{\partial^2 T}{\partial \mathrm{z}^2}\right) \quad /16/$$

where T is the temperature (K), v_i is the speed (m/s) in direction “i” and τ_{ij} is the tensor in the plane "i" with the flow in direction "j".

The generalized energy equation (Equation 16) had its velocity terms zeroed, a necessary condition when used for solids.

The software used to build the geometry, production of the mesh, resolution of the equations, and obtaining the results was the Ansys CFX® 17.0 (*31*). The solutions were considered to have converged at the time when the normalizing residue (RMS) was less than $1{\cdot}10^{-4}$ (*28*).

RESULTS AND DISCUSSION

Drying kinetics

The dying kinetics data, conducted under different temperature conditions used, are presented in Fig. 2, where the Y-axis (X_θ) is in the logarithmic scale. At 50 ºC (Fig. 2a), the treatments US20 and US30 resulted in a shorter time to reach the equilibrium condition (180 min), followed by the US10 treatment (210 min). These values represent a reduction of the time obtained in the SU treatment (240 min). This reduction is on the order of 25 % for the US20/US30 treatments and 12.5 % for the US10 treatment. Concerning the kinetics at 60 ºC (Fig. 2b), the data presented a similar tendency, where the treatments US20 and US30 also had the shortest time to reach equilibrium (120 min) followed by US10 (150 min) and SU (180 min). It was also observed the kinetics at 70 ºC (Fig. 2c), where it was necessary 90 min (US20/US30), 120 min (US10), and 150 min (SU).

Fig. 2d shows the percentage reductions in drying time concerning the SU treatment for the US10 and US20 treatments at the different temperatures studied. A synergistic effect was observed between the type of treatment and temperature causing the percentage of reduction in the drying time, when comparing the treatments US and SU, to increase with temperature and exposure time to ultrasound. Nowacka *et al.* (*32*) reported similar results, obtaining reductions of 31-40 % in the apple drying time at 70 °C, air velocity of 1.5 m/s, and frequency of 35 kHz, applying ultrasound for 10, 20, and 30 min. However, it is also possible to find studies in which the increase in temperature promotes a reduction in drying time reduction (*8,33*). This difference, linked to the chaos of the microstructural rearrangement of the product, is best explained below.

Empirical modelling of experimental kinetics

Table 1 presents the results of the adjustment of the empirical models (Page, Two terms, and Henderson and Pabis) to the experimental data obtained. For all the studied conditions, the models presented satisfactory R^2 values, being the Two terms model, together with Page model, those that had the best fit, under all conditions when compared to the Henderson and Pabis model. The best suitability of one model over another in the empirical modeling of drying kinetics can be explained by their dependence on operating conditions and characteristics of the material matrix, as observed in different works reported in the literature (*7, 34-37*).

Despite the high R^2 obtained in the Henderson and Pabis model, it presented percentage errors varying 35.46-58.16 %, which is justified by the distribution of the data along the regression line since the error variance is constant throughout the studied range, that is, the observed responses show homoscedasticity (*38*). Such behavior was not observed in the Two terms and Page models, which presented low percentage errors. Fig. 3 shows the fitting of the Two terms model, which had the smallest error.

Mass transfer in terms of effective diffusivity (D_{eff})

The values referring to the variation of the effective diffusivity with the change of temperature, obtained through the Fick Equation, are presented in Table 2. The increase of the exposure time to the ultrasonic waves caused an increase in the diffusivity for all conditions. The application of ultrasound facilitates the exit of water, increasing its diffusivity, as emphasized by Zhang *et al.* (*37*), which analyzed the effect of ultrasound on mass transfer and water removal from mushroom slices. However, this effect did not show when drying US30 samples at 60 °C. In this operating condition, the increase in ultrasound time from 20 (US20) to 30 (US30) minutes reduced the diffusivity by 4.42 %. This peculiar phenomenon, associated with the different temperature effects on the drying time observed in the literature, shows that the microstructural rearrangement of the product is chaotic after exposure to the ultrasonic waves. Thus, it can be unpredictable the consequences on the effective diffusivity, depending on the operating temperature range, since the structure can be organized in a way that will benefit or hinder the water transport of water from the interior to the external medium of the product. Other research studies reported similar behavior. Nowacka *et al.* (*32*), evaluating the effect of ultrasound application on apple drying, found that the application of 10 min of ultrasound resulted in a higher diffusivity coefficient than the treatment with 20 min, generating a percentage difference of 5.07 %. Romero and Yépez (*39*), studying the effect of ultrasound as a pretreatment to Andean blackberry (*Rubus glaucus* Benth) convective drying, noticed that at an air velocity of 3 m/s and 50 °C, the increase of the ultrasound application time from 10 to

30 min caused a reduction of the effective diffusivity of the water in the order of 1.25 %. Corrêa *et al.* (*6*), studying the influence of ultrasound application on osmotic pre-treatment and subsequent drying of pineapple, also observed a decrease in diffusivity as the time of exposure of the ultrasound increased, at temperatures of 40 ºC (6.70 %) and 70 ºC (2.86 %).

Fig. 4 shows the linear profile of the diffusivity with the inverse of the temperature, based on Table 2. The data presented a good fit, obtaining R^2> 0.994 for SU and US10 treatments, and R^2> 0.977 for treatments US20 and US30. Tzempelikos *et al.* (*19*) found similar R^2 values, around 0.98.

Mass transfer in terms of water loss (WL) and solids gain (SG)

Two parameters used to determine the condition for CFD simulation were analyzed: WL (%) and SG (%), and their obtained values are presented in Table 2. The obtained negative WL values (%) indicated a water gain in all the treatments. As regarding SG (%), the values obtained were also negative, that is, there was a loss of solids. These behaviors corroborate with that found in other studies involving ultrasonic pretreatment in fruit dehydration. Fernandes and Rodrigues (*24*), for sapota (*Achras sapota* L.) drying, found values ranging from -4.0 to -5.2 % and -2.7 to -7.8 % for WL (%) and SG (%), respectively. Garcia-Noguera *et al.* (*40*) obtained values ranging from -2.7 to -3.9 % for WL (%) and from -0.1 to -0.7 % for SG (%) for strawberry dehydration. Silva *et al.* (*10*), in the drying of melon slices, obtained values in the range -8.51 to -10.59 % and -0.07 to -1.45 %, for WL and SG, respectively.

The treatments US20 and US30 provided higher reductions in drying time when comparing to SU. As these reductions were similar between the two treatments, the use of water loss and solids gain parameters was important for determining an adequate condition. The condition used for simulation was the treatment US20 at 60 °C since water gain (negative WL) was lower in the US20 treatment than in the US30, and this was the determining factor for the choice, as SG values for the two treatments were closer and relied on the dry basis of the product, representing a small fraction of the total mass. The kinetic and diffusion data (Table 2) also corroborated to the choice of the US20 treatment at 60 °C for the condition for simulation.

Simulation via CFD of the temperature profile on the melon slice

The values of the properties used in the temperature profile simulation of the melon slice were: k_p (W/m·K) = 0.5849 (SU) and 0.5953 (US20); C_p (J/kg·K) = 3891.830 (SU) and 3954.830 (US20); ρ (kg/m^3) = 2028.467 (SU) and 2055.224 (US20).

Figure 5 presents the temperature profile of the solid phase of the moist melon, over time, for US20/60 °C treatment. There was also a simulation for SU/60 °C condition. However, the profile

obtained was similar to that of the US20/60 ºC, and not shown in this work. The geometry was considered unchanged throughout the two processes, and there was only a small difference between the local temperatures when comparing the two treatments since the values of C_p, k_P, and ρ were subtly smaller in SU/60 ºC.

The results presented in Fig. 5 show that the temperature is higher at the edges since the proposed geometry generates turbulence in these regions, which in turn increases the local heat transfer coefficient. As it moves away from the lateral zones towards the center, a decrease in temperature is observed. This is due to the low-pressure regions formed above the melon (Fig. 6a), due to the vortices generated by lateral air flows (Fig. 6b), reducing the local heat transfer coefficients (*41*). The literature reports similar behavior on temperature profile generated by numerical methods for fruits and moist objects (*19-21*).

CONCLUSIONS

The drying kinetics results showed that applying ultrasound as a pretreatment offered a positive synergy with temperature. The longer the exposure time to ultrasound, together with the increase in drying temperature, the longer the drying time reduction, reaching up to 40 % at 70 °C decrease with the application of ultrasound for 20 min. The empirical model that presented the best fit to the experimental drying data was the Exponential Two terms, obtaining $R^2 > 0.999$ and percentage errors of less than 12 %. Regarding diffusivity, there was a dependence on temperature following the Arrhenius equation. The effective diffusivity coefficient showed a tendency to increase as the melon exposure time to ultrasonic waves increased. However, at 60 °C, a peculiarity was observed regarding this tendency, since, by increasing the ultrasound time from 20 to 30 min, the effective diffusivity decreased rather than increased. The values of WL (%) and SG (%) were used, together with the kinetic and diffusive data, to choose the best pretreatment condition for CFD simulation. The results of the CFD simulation for the temperature distribution along the melon slices were consistent with the data found in the literature. Therefore, the profile obtained satisfactorily describes the drying process.

ACKNOWLEDGMENTS

The authors gratefully acknowledge UFPE (Universidade Federal de Pernambuco), CNPq (Conselho Nacional de Desenvolvimento Científico e Tecnológico) and CAPES (Coordenação de Aperfeiçoamento de Pessoal de Nível Superior) for the fellowships.

AUTHORS' CONTRIBUTION

JHF Silva contributed with the conception of the work, investigation, methodology, data collection, data analysis and interpretation, critical revision, writing, final approval of the version to be published.

JS Silva Neto assisted in writing, critical reviews, discussion of concepts, data analysis.

ES Silva contributed with data collection, writing, critical reviews.

DES Cavalcanti contributed with the conception of the work, discussion of concepts, methodology, critical reviews.

PM Azoubel performed the conception of the work, data analysis and interpretation, critical revision, writing, supervision, final approval of the version to be published, funding acquisition.

M Benachour performed the conception of the work, data analysis and interpretation, critical revision, writing, supervision, funding acquisition.

ORCID ID

JHF Silva https://orcid.org/0000-0003-3448-2565

JS Silva Neto https://orcid.org/0000-0001-8521-7804

ES Silva https://orcid.org/0000-0002-5403-7461

DES Cavalcanti https://orcid.org/0000-0003-4795-4058

PM Azoubel https://orcid.org/0000-0001-9890-5294

M Benachour https://orcid.org/0000-0003-0139-9888

REFERENCES

1. Cârlescu P-M, Arsenoaia V, Roşca, R, Ţenu, I. CFD simulation of heat and mass transfer during apricots drying. LWT – Food Sci Technol. 2017; 85(Part B):479–86. https://doi.org/10.1016/j.lwt.2017.03.015

2. Vilela CAA, Artur PO. Drying of saffron (*Curcuma longa* L.) in different geometric cuts. Ciênc Tecnol Alime. 2008; 28(2):387–94 (in Portuguese). https://doi.org/10.1590/S0101-20612008000200018

3. Jin W, Zhang M, Shi W. Evaluation of ultrasound pretreatment and drying methods on selected quality attributes of bitter melon (*Momordica charantia* L.). Dry Technol. 2019;37(3) 387–96. https://doi.org/10.1080/07373937.2018.1458735

4. Cao X, Zhang M, Mujumdar AS, Zhong Q, Wang Z. Effects of ultrasonic pretreatments on quality, energy consumption and sterilization of barley grass in freeze-drying. Ultrason Sonochem. 2018;40(Part A):333–40.
https://doi.org/10.1016/j.ultsonch.2017.06.014

5. Wang L, Xu B, Wei B, Zeng R. Low frequency ultrasound pretreatment of carrot slices: Effect on the moisture migration and quality attributes by intermediate-wave infrared radiation drying. Ultrason Sonochem. 2018; 40(Part A):619–28.
https://doi.org/10.1016/j.ultsonch.2017.08.005

6. Corrêa JLG, Rasia MC, Mulet A, Cárcel JA. Influence of ultrasound application on both the osmotic pretreatment and subsequent convective drying of pineapple (*Ananas comosus*). Innov Food Sci Emerg. 2017;41:284–91.
https://doi.org/10.1016/j.ifset.2017.04.002

7. Horuz E, Jaafar HJ, Maskan M. Ultrasonication as pretreatment for drying of tomato slices in a hot air–microwave hybrid oven. Dry Technol. 2017;35(7):849–59.
https://doi.org/10.1080/07373937.2016.1222538

8. Magalhães ML, Cartaxo SJM, Gallão MI, García-Pérez JV, Cárcel JA, Rodrigues S, Fernandes FAN. Drying intensification combining ultrasound pre-treatment and ultrasound-assisted air-drying. J Food Eng. 2017;215:72–77.
https://doi.org/10.1016/j.jfoodeng.2017.07.027

9. Oladejo AO, Ma H, Qu W, Zhou C, Wu B, Yang X, Onwude DI. Effects of ultrasound pretreatments on the kinetics of moisture loss and oil uptake during deep fat frying of sweet potato (*Ipomea batatas*). Innov. Food Sci. Emerg. 2017;43:7–17.
https://doi.org/10.1016/j.ifset.2017.07.019

10. Silva, GD, Barros ZMP, Medeiros RAB, Carvalho CBO, Brandão SCR, Azoubel PM. Pretreatments for melon drying implementing ultrasound and vacuum. LWT – Food Sci Technol. 2016;74:114–19.
https://doi.org/10.1016/j.lwt.2016.07.039

11. Tao Y, Wang P, Wang Y, Kadam SU, Han Y, Wang J, Zhou J. Power ultrasound as a pretreatment to convective drying of mulberry (*Morus alba* L.) leaves: Impact on drying kinetics and selected quality properties. Ultrason Sonochem. 2016;31:310–18.
https://doi.org/10.1016/j.ultsonch.2016.01.012

12. Musielak G, Mierzwa D, Kroehnke J. Food drying enhancement by ultrasound – A review. Trends Food Sci Tech. 2016;56:126–41.
https://doi.org/10.1016/j.tifs.2016.08.003

13. Powles AE, Martin DJ, Wells IT, Goodwin CR. Physics of ultrasound. Anaesth Intens Care. 2018;19(4):202–05.
https://doi.org/10.1016/j.mpaic.2018.01.005
14. Ekezie F-GC, Cheng J-H, Sun D-W. Effects of nonthermal food processing technologies on food allergens: A review of recent research advances. Trends Food Sci Tech. 2018;74:12–25.
https://doi.org/10.1016/j.tifs.2018.01.007
15. Başlar M, Toker ÖS, Karasu S, Tekin ZH, Yildirim HB. Handbook. Ultrason Sonochem. Singapore: Springer Singapore. 2016.
https://doi.org/10.1007/978-981-287-278-4
16. Defraeye T, Radu A. Convective drying of fruit: A deeper look at the air-material interface by conjugate modeling. Int J Heat Mass Trans. 2017;108(Part B):1610–22.
https://doi.org/10.1016/j.ijheatmasstransfer.2017.01.002
17. Wang B, Yao M. Examination of drying behavior of mung bean in laboratory and the establishment of the corresponding REA model. J Food Proc Pres. 2017;41(3):1–8.
https://doi.org/10.1111/jfpp.12939
18. Darabi H, Zomorodian A, Akbari MH, Lorestani AN. Design a cabinet dryer with two geometric configurations using CFD. J Food Sci Technol. 2015;52(1):359–66.
https://doi.org/10.1007/s13197-013-0983-1
19. Tzempelikos DA, Mitrakos D, Vouros AP, Bardakas AV, Filios AE, Margaris DP. Numerical modeling of heat and mass transfer during convective drying of cylindrical quince slices. J Food Eng. 2015;156:10–21.
https://doi.org/jfoodeng.2015.01.017
20. Villa-Corrales L, Flores-Prieto JJ, Xamán-Villaseñor JP, García-Hernández E. Numerical and experimental analysis of heat and moisture transfer during drying of Ataulfo mango. J Food Eng. 2010;98(2):198–206.
https://doi.org/10.1016/j.jfoodeng.2009.12.026
21. Chandra Mohan VP, Talukdar P. Three-dimensional numerical modeling of simultaneous heat and moisture transfer in a moist object subjected to convective drying. Int J Heat Mass Trans. 2010;53:4638–50.
https://doi.org/10.1016/j.ijheatmasstransfer.2010.06.029
22. Tu J, Yeoh G-H, Liu C. CFD Techniques: The Basics. In: Computational Fluid Dynamics. Elsevier. 2018;155–210.
https://doi.org/10.1016/B978-0-08-101127-0.00005-2

23. AOAC. Official methods of analysis of AOAC. Method 934.06. Fruits and Fruit Products/Dried Fruit. International 17th edition; Gaithersburg, MD, USA Association of Analytical Communities. 2000. Available from: http://www.eoma.aoac.org/methods/info.asp?ID=21670.

24. Fernandes FAN, Gallão MI, Rodrigues S. Effect of osmotic dehydration and ultrasound pre-treatment on cell structure: Melon dehydration. LWT – Food Sci Technol. 2008;41(4):604–10. https://doi.org/10.1016/j.lwt.2007.05.007

25. Crank J. The diffusion equations. In: The mathematics of diffusion. 2. ed. London: Oxford University Press. 1975. https://doi.org/10.1088/0031-9112/26/11/044

26. Başlar M, Kiliçli M, Yalinkiliç B. Dehydration kinetics of salmon and trout fillets using ultrasonic vacuum drying as a novel technique. Ultrason Sonochem. 2015;27:495–502. https://doi.org/10.1016/j.ultsonch.2015.06.018

27. TIBCO Statistica, v. 10, TIBCO Software Inc, 2010. Available from: https://www.tibco.com/

28. Sajjadi B, Asgharzadehahmadi S, Asaithambi P, Raman AAA, Parthasarathy R. Investigation of mass transfer intensification under power ultrasound irradiation using 3D computational simulation: A comparative analysis. Ultrason Sonochem. 2017;34:504-18. https://doi.org/10.1016/j.ultsonch.2016.06.026

29. Tu J, Yeoh G-H, Liu C. CFD Mesh Generation: A Practical Guideline. In: Computational Fluid Dynamics. Elsevier. 2018;125–54. https://doi.org/10.1016/B978-0-08-101127-0.00004-0

30. Ansys Help. CFX: Theory Guide, Ansys Inc., 2017. https://www.ansys.com/

31. ANSYS CFX, v. 17, ANSYS Inc, 2017. Available from: https://www.ansys.com/

32. Nowacka M, Wiktor A, Śledź M, Jurek N, Witrowa-Rajchert D. Drying of ultrasound pretreated apple and its selected physical properties. J Food Eng. 2012;113(3):427–33. https://doi.org/10.1016/j.jfoodeng.2012.06.013

33. Rodríguez Ó, Santacatalina JV, Simal S, Garcia-Perez JV, Femenia A, Rosselló C. Influence of power ultrasound application on drying kinetics of apple and its antioxidant and microstructural properties. J Food Eng. 2014;129:21–9. https://doi.org/10.1016/j.jfoodeng.2014.01.001

34. Kadam SU, Tiwari BK, O'Donnell CP. Effect of ultrasound pre-treatment on the drying kinetics of brown seaweed Ascophyllum nodosum. Ultrason Sonochem. 2015 23:302–07. https://doi.org/10.1016/j.ultsonch.2014.10.001

35. Méndez EK, Orrego CE, Manrique DL, Gonzalez JD, Vallejo D. Power Ultrasound Application on Convective Drying of Banana (*Musa paradisiaca*), Mango (*Mangifera indica* L.) and Guava (*Psidium guajava* L.). Int J Agric Biol. Eng. 2015;9:973–78.
https://publications.waset.org/10002639/pdf

36. Ricce C, Rojas ML, Miano AC, Siche R, Augusto, PED. Ultrasound pre-treatment enhances the carrot drying and rehydration. Food Res Int. 2016;89(Part 1):701–8.
https://doi.org/10.1016/j.foodres.2016.09.030

37. Zhang Z, Liu Z, Liu C, Li D, Jiang N, Liu, C. Effects of ultrasound pretreatment on drying kinetics and quality parameters of button mushroom slices. Dry Technol. 2016;34(15):1791–1800.
https://doi.org/10.1080/07373937.2015.1117486

38. Barros Neto B, Scarminio IS, Bruns RE. Como fazer experimentos: Pesquisa e desenvolvimento na ciência e na indústria. Campinas, SP: Editora da Unicamp. 2001.

39. Romero J CA, Yépez V BD. Ultrasound as pretreatment to convective drying of Andean blackberry (*Rubus glaucus Benth*). Ultrason Sonochem. 2015;22:205–10.
https://doi.org/10.1016/j.ultsonch.2014.06.011

40. Garcia-Noguera J, Oliveira FIP, Gallão MI, Weller CL, Rodrigues S, Fernandes FAN. Ultrasound-assisted osmotic dehydration of strawberries: Effect of pretreatment time and ultrasonic frequency. Dry Technol. 2010;28(10):294–303.
https://doi.org/10.1080/07373930903530402

41. Bejan, A. Convection Heat Transfer. Hoboken, NJ, USA: John Wiley & Sons, Inc. 2013.
https://doi.org/10.1002/9781118671627

Table 1. R^2 for Page (Pg), Two terms (TT) and Henderson and Pabis (HP) models for different food matrices drying kinetics data fittings, and models' parameters and percentage errors (E) for melon drying

Treatment	Parameters	Temperature/°C								
		50			60			70		
		TT	HP	Pg	TT	HP	Pg	TT	HP	Pg
SU	*a*	0.7353	0.9921	-	0.6638	0.9955	-	0.6086	0.9960	-
	k	0.1115	0.0695	0.1813	0.1500	0.0838	0.2178	0.2925	0.0952	0.3211
	n	-	-	0.6886	-	-	0.6781	-	-	0.5826
	w	0.0272	-	-	0.0395	-	-	0.0444	-	-
	R^2	0.9999	0.9963	0.9999	0.9999	0.9976	0.9999	0.9999	0.9964	0.9999
	E/%	1.16	35.46	5.21	1.75	41.74	1.81	0.57	38.60	0.63
US10	*a*	0.7377	0.9910	-	0.7223	0.9947	-	0.6253	0.9976	-
	k	0.1505	0.0779	0.3212	0.1708	0.0885	0.3257	0.2808	0.1044	0.3297
	n	-	-	0.5319	-	-	0.5585	-	-	0.5989
	w	0.0242	-	-	0.0317	-	-	0.0498	-	-
	R^2	0.9999	0.9919	0.9999	0.9999	0.9951	0.9999	0.9999	0.9977	0.9999
	E/%	0.56	43.29	1.16	0.40	46.83	1.79	1.46	40.76	3.96
US20	*a*	0.7367	0.9941	-	0.7092	0.9974	-	0.6335	0.9986	-
	k	0.1457	0.0829	0.2746	0.2245	0.1054	0.3840	0.3486	0.1167	0.3586
	n	-	-	0.5982	-	-	0.5490	-	-	0.6023
	w	0.0297	-	-	0.0409	-	-	0.0572	-	-
	R^2	0.9999	0.9955	0.9999	0.9999	0.9970	0.9999	0.9999	0.9986	0.9999
	E/%	0.97	43.87	2.43	1.29	51.75	1.20	0.22	43.79	4.02
US30	*a*	0.7529	0.9936	-	0.7676	0.9971	-	0.6800	0.9991	-
	k	0.1550	0.0847	0.3309	0.1735	0.1010	0.3555	0.2339	0.1206	0.3333
	n	-	-	0.5422	-	-	0.5636	-	-	0.6382
	w	0.0266	-	-	0.0345	-	-	0.0589	-	-
	R^2	0.9999	0.9940	0.9999	0.9999	0.9970	0.9999	0.9999	0.9991	0.9999
	E/%	0.72	45.75	1.43	2.31	58.16	29.34	0.60	43.49	3.14

a, *k, n*, and *w,* are the empirical constants in drying models

Table 2. Drying effective diffusivity (D_{eff}) and water loss (WL) and solids gain (SG) after ultrasonic pretreatment.

Treatment	$D_{eff} \cdot 10^9$/(m²/s)						WL/%	SG/%
	323.15 K (50 °C)	R^2	333.15 K (60 °C)	R^2	343.15 K (70 °C)	R^2		
SU	2.47	0.9965	3.00	0.9969	3.43	0.9974	-	-
US10	2.75	0.9899	3.17	0.9930	3.82	0.9964	-1.19 ±0.17	-1.61 ±0.02
US20	2.97	0.9944	3.85	0.9951	4.33	0.9974	-1.32 ±0.28	-2.20 ±0.03
US30	3.02	0.9914	3.68	0.9953	4.50	0.9983	-2.65 ±0.09	-2.30 ±0.01

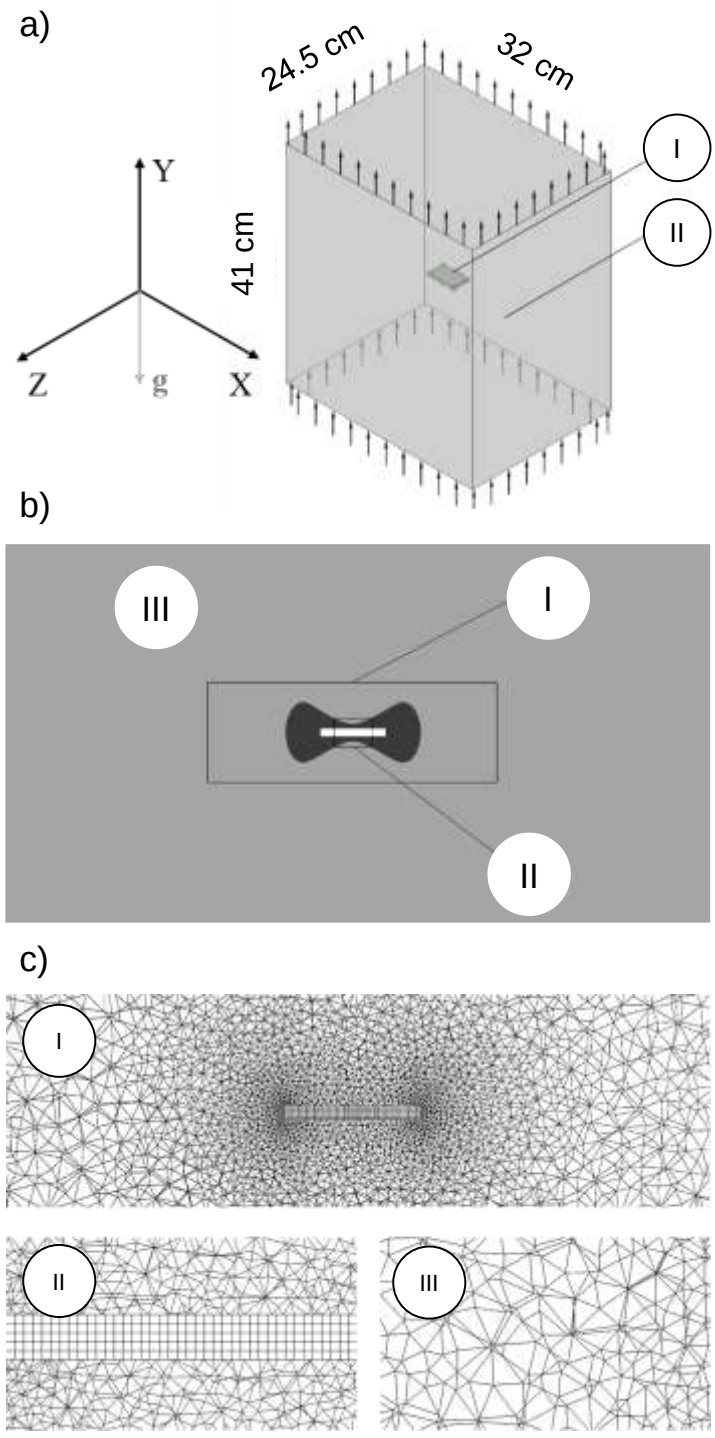

Fig. 1. a) Melon slice (I) and simplified dryer body (II). b) Representation of the structured and unstructured mesh zones used in the XY plane. c) Denser unstructured zone around of the melon (I), structured mesh zone used in the melon (II) and less denser mesh area, representing the external fluid medium (drying air) (III)

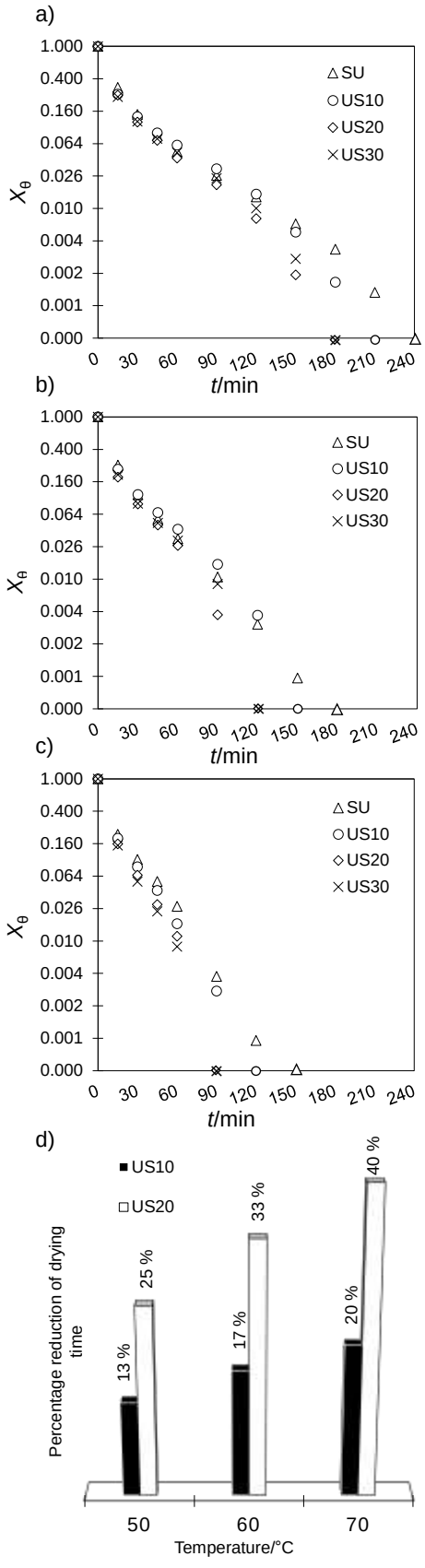

Fig. 2. Melon drying kinetics data at a) 50 °C, b) 60 °C, and c) 70 °C for different treatments and d) percentage reduction of drying time with increasing temperature for different treatments

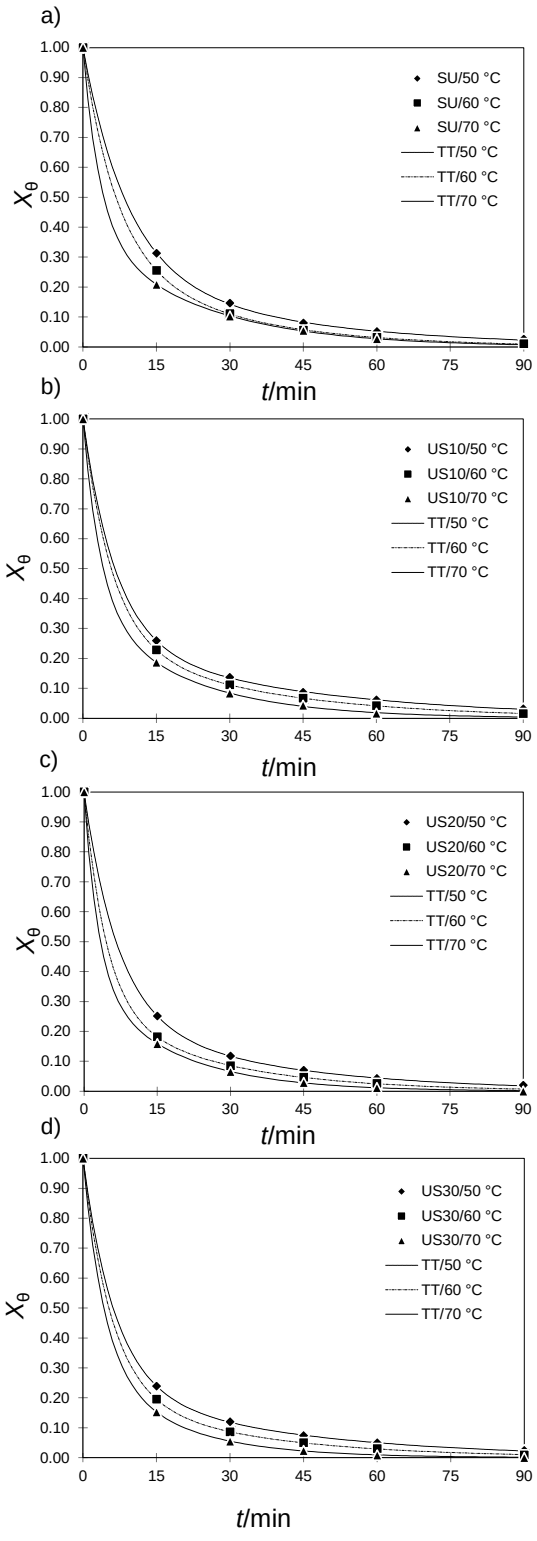

Fig. 3. Empirical modeling of experimental data for a) SU, b) US10, c) US20 and d) US30 treatments. The continuous lines represent the best adjusted model, Two-terms (TT), for the different temperatures

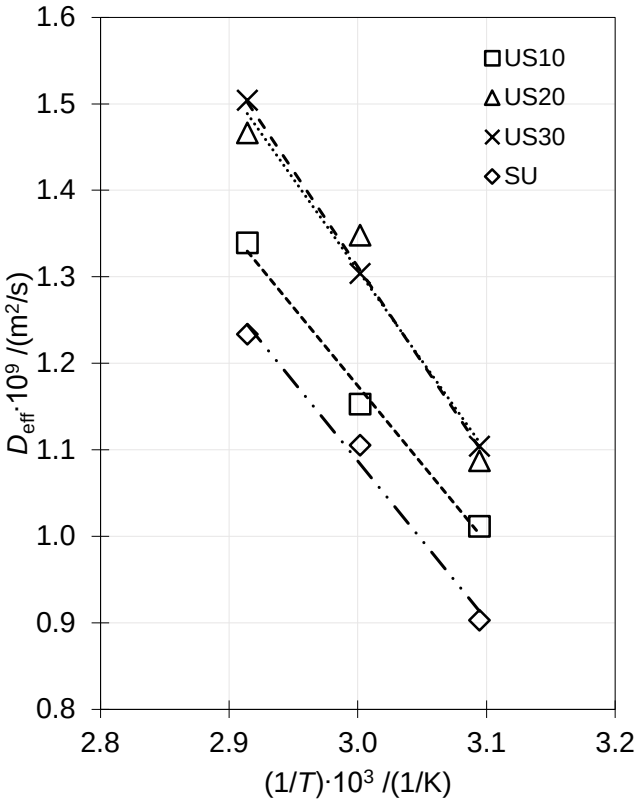

Fig. 4. Dependence of the diffusivity with the inverse of the temperature

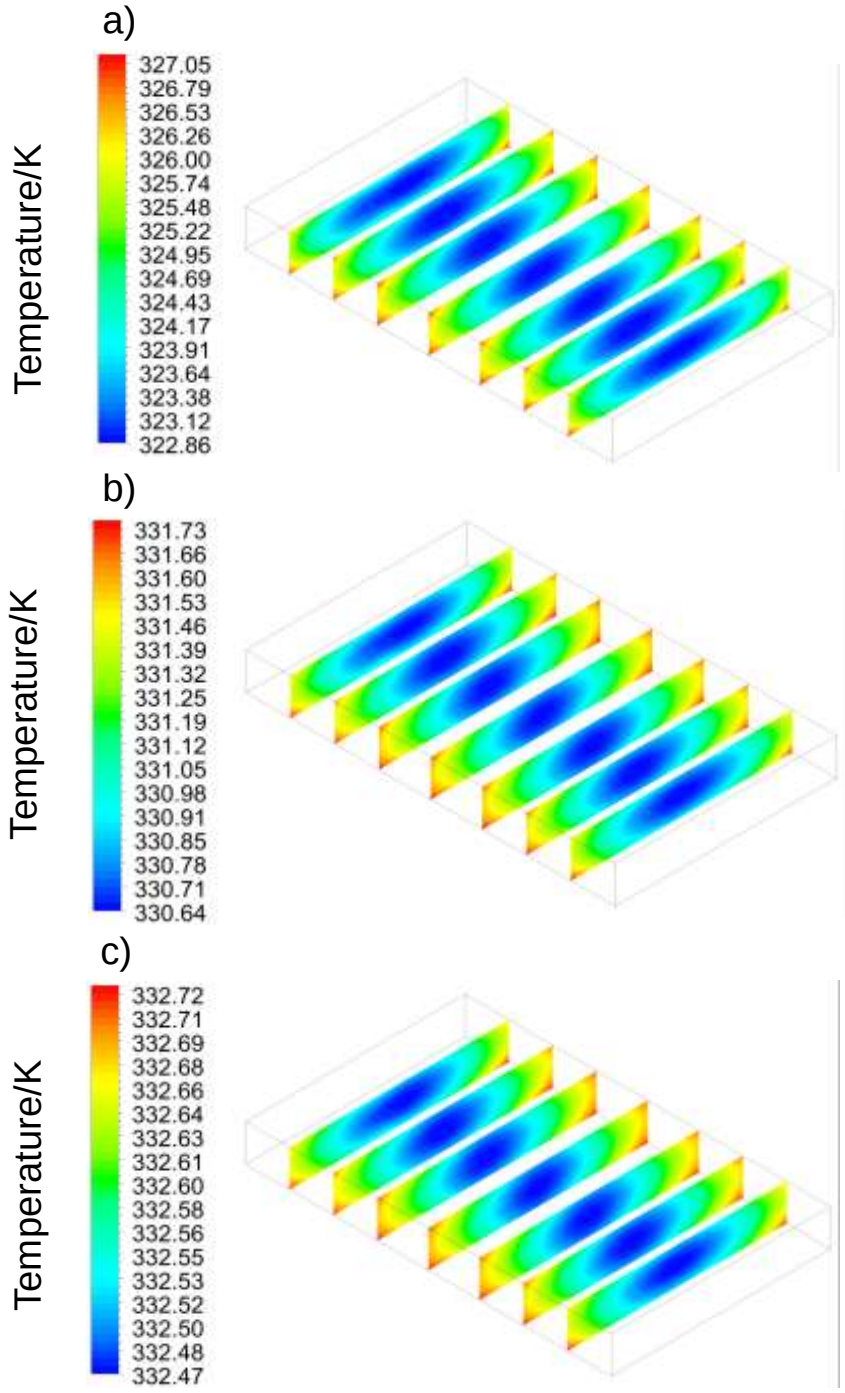

Fig. 5. Temperature profile on melon slice (US20/60 °C). Slice condition after a) 30 min, b) 60 min and c) 90 min

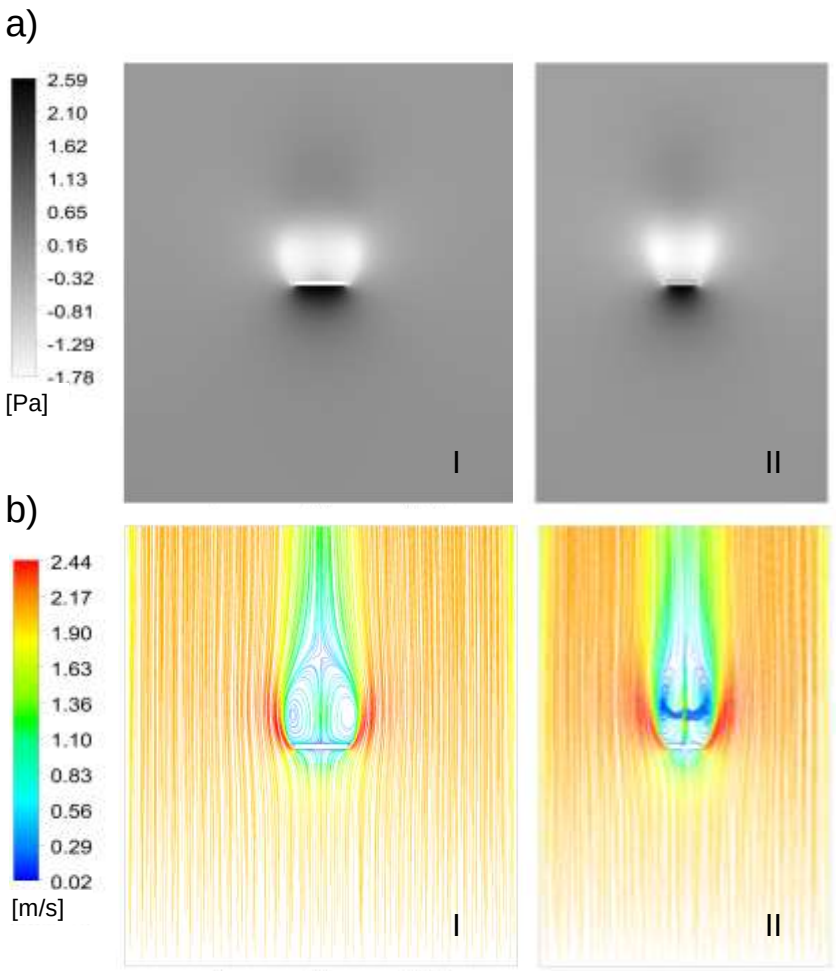

Fig. 6. Relative pressure of the a) YX (I) and YZ (II) planes. Current lines in the b) YX (I) and YZ (II) planes